Chapter 2

The Detection of Organic Pollutants at Trace Level by Variable Kinds of Silver Film with Novel Morphology

Zhengjun Zhang, Qin Zhou and Xian Zhang

Additional information is available at the end of the chapter

http://dx.doi.org/10.5772/53602

1. Introduction

In the modern world, environmental problems have attracted more and more attention, for environmental pollutants are extremely harmful to human beings' health. Environmental pollutants, such as persistent organic pollutants, are widely separated in the environment and difficult to detect at trace level.Within persistent organic pollutants, polychlorinated biphenyls (PCBs), due to their excellent dielectric properties, had been widely used since the 1920s in transformers, heat transfers, capacitors, etc., and had polluted nearly everywhere in the world [1]. In recent years, however, they have been found to be very harmful to human beings. They may cause serious diseases, such as cancers and gene distortion, when exceeding the critical dose in human bodies, and more seriously, PCBs can be accumulated in plants and animals from the environment and yield higher doses in human bodies, making PCBs very dangerous to human beings even in trace amounts [1-3]. Therefore, the detection of PCBs in trace amounts is crucial. Currently, the mostly applied detection technique for PCBs is the combination of high-resolution gas chromatography and mass spectrometry. It requires, however, very sophisticated devices, standard samples, complicated pretreatments of samples, favourable experimental environments and experienced operators [4-7]. Thus, new methods are demanded especially for the rapid detection of trace amounts of PCBs.

Surface-enhanced Raman scattering (SERS) has been proven to be an effective way to detect some organics [8]. With the great progress of nanoscale technology in recent years, SERS has attracted enormous attention due to its excellent performance and potential applications in the detection of molecules in trace amounts, even single molecule detection.

Among the approaches so far available to prepare nanostructure as SERS substrate, the glancing angle deposition (GLAD) technique is a simple but powerful means which is capable of producing thin films with pre-designed nanostructures. These nanostructures can be

used in the field of SERS. For instance, using Ag nanorods as SERS substrates,Rhodamine 6G with concentration of 10^{-14} M (dissolved in water) was detected [9]; with the alumina-modified AgFON substrates, bacillus subtilis spores were detected to 10^{-14} M [10, 11]; Vo-Dinh reported even the detection of specific nucleic acid sequences by the SERS technique [12-14]. In spite of the numerous studies on the application as a chemical and biological sensor [15-17], the SERS technique has not yet been employed to detect PCBs as they are hardly dissolved in water.

2. Fabrication ofsilver nanostructure as sensitive SERS substrates

The detection sensitivity of SERS depends considerably on the surface property of the SERS substrate. High aspect ratio, nanostructured Ag, Au, Cu substrates are proved to be good SERS substrates. For instance, using ordered arrays of gold particles prepared through a porous alumina template as the SERS substrate, Rhodamine 6G (R6G) molecules were detected to a concentration limit of 10^{-12} M; arrays of silicon nanorods coated with thin films of Ag served as good SERS substrates for R6G molecule detection, etc [12, 16]. Thus the preparation of SERS substrates with preferred surface property is of great importance. There are several methods to prepare these kinds of SERS substrates and in this chapter we take glancing angle deposition as an example.

Glancing angle deposition (GLAD) technique is a simple but powerful means of producing thin films with pre-designed nanostructures, such as nanopillars, slanted posts, zigzag columns and spirals. Silver nanorod arrays prepared by GLAD are excellent SERS substrates.

In addition, the SERS properties are related to the optical properties of the nanorod arrays. Both SERS properties and optical properties depend on the structure of the nanorods, such as the shape, length, separation, tilting angle and so on, which can be tuned by the deposition conditions.

2.1. Fabrication of sensitive SERS substrates by GLAD

The detection sensitivity of the SERS technique depends greatly on the surface property of the SERS substrate [45,46]. Among the approaches so far available to prepare nanostructured materials, the glancing angle deposition (GLAD) technique is a simple but powerful means of producing thin films with pre-designed nanostructures [47-48], such as nanopillars, slanted posts, zigzag columns, spirals [18-19], etc [20-23]. For example, arrays of Ag nanorods were found to be good SERS substrates for the detection of trans-1,2-bis(4-pyridyl)ethane molecules, with a SERS enhancement factor greater than 10^8 [16]. It is therefore of great interest to investigate the growth of metal nanostructures by the GLAD technique [49].

Pristine Si wafers with (001) orientation were used as substrates. These were supersonically cleaned in acetone, ethanol and de-ionized water baths in sequence, and were fixed on the GLAD substrate in an e-beam deposition system. The system was pumped down to a vacuum level of 3×10^{-5} Pa and then the thin Ag film was deposited on the substrate with a de-

http://dx.doi.org/10.5772/53602

positing rate of 0.5 nm/s, with the thickness monitored by a quartz crystal microbalance. To produce films of aligned Ag nanorods, the incident beam of Ag flux was set at ~ 85 ° from the normal of the silicon substrate, at different substrate temperatures. The morphology and structure of the thin Ag films was characterized by scanning electron microscope (SEM), transmission electron microscope (TEM) and high-resolution TEM, selected area diffraction (SAD) and X-ray diffraction (XRD), respectively. The performance of the nanostructured Ag films as SERS substrates was evaluated with a micro-Raman spectrometer using R6G as the model molecule.

It is well known that the major factors influencing the growth morphology of the films by GLAD are the incident direction of the depositing beam flux, the temperature and the movement of the substrate, and the deposition rate, etc. When fixing the incident Ag flux at ~85 ° from the normal of the substrate and the deposition rate at ~0.5 nm/s, the growth morphology of the Ag films was greatly dependent on the temperature and movement of the substrate. Fig 1 shows the growth morphology of thin Ag films versus the temperature and movement of the substrate. The SEM micrographs were taken by a FEI SEM (QUANTA 200FEG) working at 20 kV.

Fig 1(a) and (b) shows typical SEM images of the surface morphology of thin Ag films deposited at 120 °C, without substrate rotation and with substrate rotation at a speed of 0.2 rpm, respectively. One sees from the images that at this temperature, Ag nanorods formed in two films with a length of 500 nm, yet they were not well separated - most nanorods were joined together. A major difference between the two is the growth direction of the joined nanorods, i.e. without rotation the nanorods grew at a glancing angle on the substrate, while with substrate rotation the nanorods grew vertically aligned. Another difference noticeable is the size of the nanorods, i.e. nanorods grown with substrate rotation have a slightly larger diameter.

Fig 1(c) and (d) shows respectively the surface morphology of thin Ag films deposited at -40 °C, without substrate rotation and with rotation at a speed of 0.2 rpm. Comparing with Figs 1(a) and (b), it can be seen that the decrease in the deposition temperature led to the separation of Ag nanorods in the two films, while the rotation of the substrate also determined the growth direction and diameter of the nanorods, as observed from Figs 1(a) and 1(b). The Ag nanorods grown at this temperature are 20-30 nm in diameter, ~ 800 nm in length and are well separated. Therefore, through adjusting the temperature and movement of the substrate one can grow well separated and aligned Ag nanorods on planar silicon substrates.

Fig 1(e) and 1(f) shows respectively a bright-field TEM and a HRTEM image of Ag nanorods shown by Fig 1(c); inset of Fig 1(f) is the corresponding SAD pattern. The images and the SAD pattern were taken with a JEM-2011F working at 200 kV. One sees from the Figs that the Ag nanorod is ~ 30 nm in diameter and its micro-structure is single crystalline. By indexing the SAD pattern it is noticed that during the growth process the {111} plane of the nanorod was parallel to the substrate surface, with its axis along the <110> direction. This was confirmed by XRD analysis. Fig 2 shows a XRD pattern of the Ag nanorods shown by Fig 1(c). The pattern was taken with a Rigaku X-ray diffractometer using the Cu k. line, working at the θ-2θ coupled scan mode. From the Fig, a very strong (111) texture is observed,

indicating that the {111} plane of the Ag nanorods was parallel to the substrate surface. These suggest that one can produce arrays of aligned, single crystalline Ag nanorods by the GLAD technique even at a low substrate temperature, i.e. -40 °C.

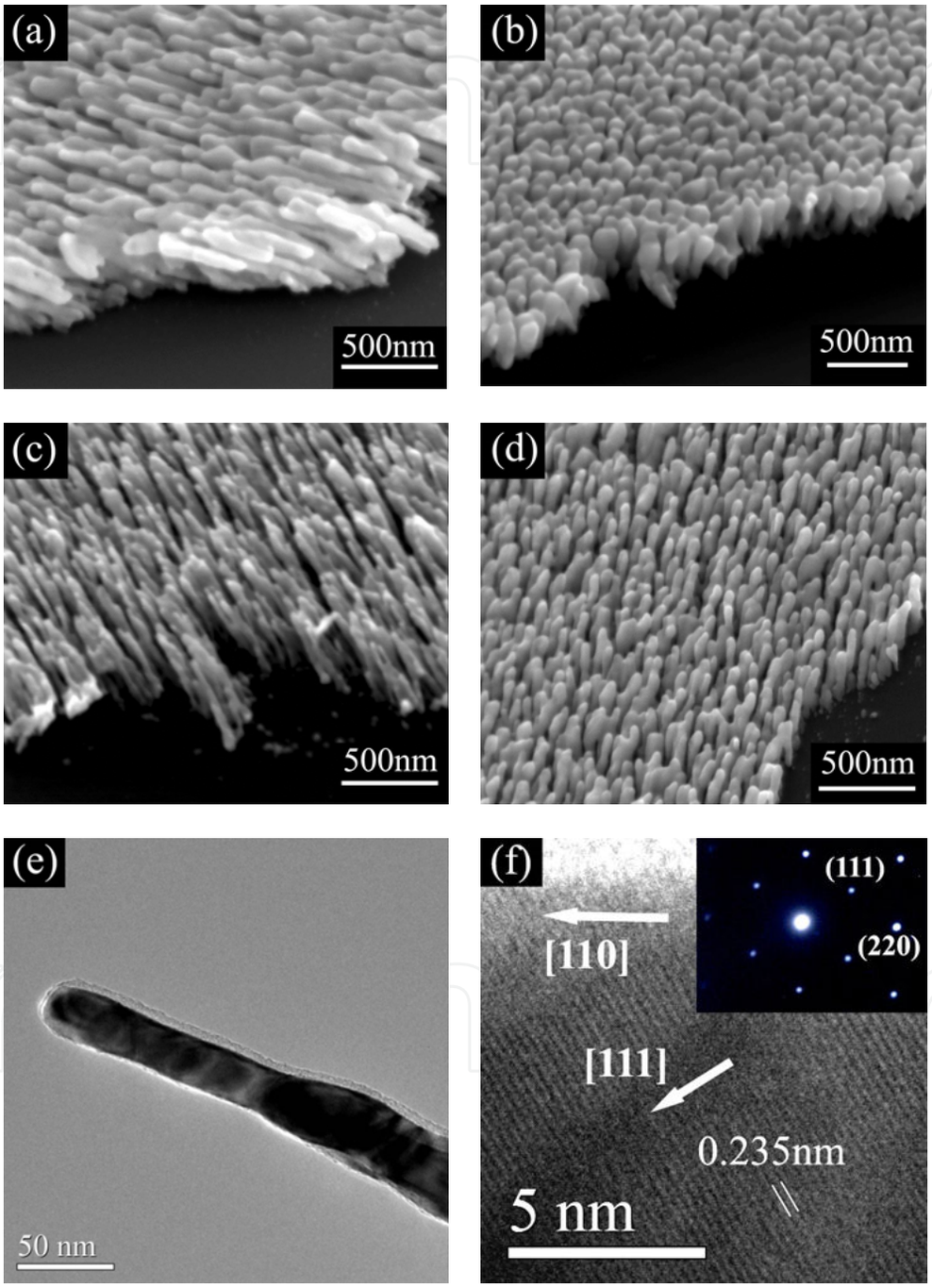

Figure 1. Growth morphology of thin Ag films by GLAD at various conditions. (a) at 120 °C without substrate rotation; (b) at 120 °C and substrate rotation at 0.2 rpm; (c) at -40 °C without substrate rotation; and (d) at -40 °C and substrate rotation at 0.2 rpm. (e) and (f) shows respectively a bright-field TEM and a HRTEM image of the nanorods shown by Fig 1(c); inset of (f) is the corresponding SAD pattern.

http://dx.doi.org/10.5772/53602

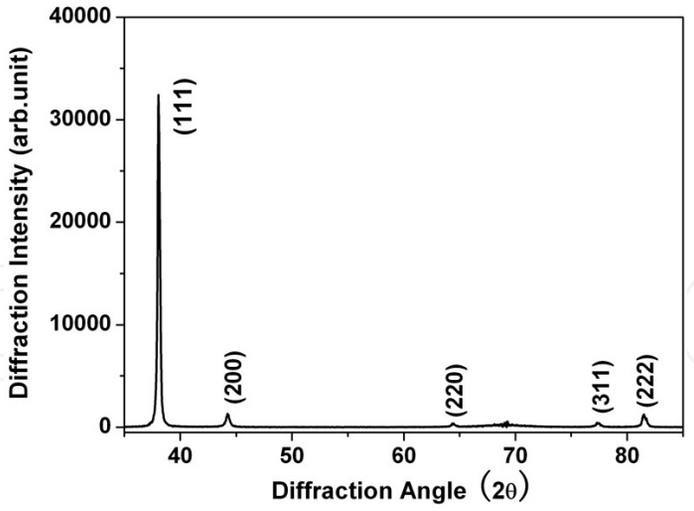

Figure 2. A XRD pattern of the Ag film consisting of well separated, single crystalline nanorods shown by Fig 1(c).

By using Rhodamine 6G as the model molecule, the performance of thin Ag films shown by Figs 1(a)-(d) is examined as the SERS substrates. These samples were dipped in a 1×10^{-6}mol/L solution of R6G in water for 30 minutes and dried with a continuous gentle nitrogen blow. Fig 3(a) and 3(b) show Raman spectra of R6G obtained on the four nanostructured Ag films by a Reinshaw 100 Raman spectrometer using a 514 nm Ar^{+} laser as the excitation source. It is observed that with the thin Ag films as the SERS substrate, all spectra exhibit clearly the characteristic peaks of R6G molecules, at 612, 774, 1180, 1311, 1361, 1511, 1575 and 1648 cm^{-1}, respectively12.However, the intensity of the Raman peaks was dependent on the morphology of the films. It is noticed that on Ag films consisting of well separated nanorods, see Figs 3(b), the Raman peaks of R6G are much stronger than those on films of joined nanorods, see Figs 3(a). This suggests that arrays of aligned but well separated Ag nanorods represent excellent SERS performance.

Using arrays of aligned Ag nanorods shown by Figs 1(c) and 1(d) as SERS substrates, we examined the detection limit of R6G molecules in water by the SERS technique. Fig 4(a) shows Raman spectra of R6G obtained on Ag nanorods shown by Fig 1(c), as a function of the concentration of R6G in water ranging from 1×10^{-8} to 1×10^{-16}mol/L. Similar results were also obtained for Ag nanorods shown by Fig 1(d). The Raman spectra were obtained by one scan with an accumulation time of 10 s, at a laser power of 1 % to avoid decomposition of R6G. It is found that characteristic peaks of R6G were all observed at all concentrations. To clearly show this, we plot the Raman spectrum at 10^{-14}mol/L in Fig 4(b). It is noticed that although the intensity of the peaks is almost two orders lower than that at 10^{-6}mol/L, the spectrum contains the clear characteristic peaks of R6G12. These suggest that Ag films consisting of aligned and well separated Ag nanorods with single crystalline could serve as excellent SERS substrate for trace amount detection of R6G molecules. However, in the Raman spectrum at 10^{-16}mol/L in Fig 4(a), some of the peaks of R6G disappear. That suggests the concentration limit of this method is 10^{-14}mol/L in the authors' work.

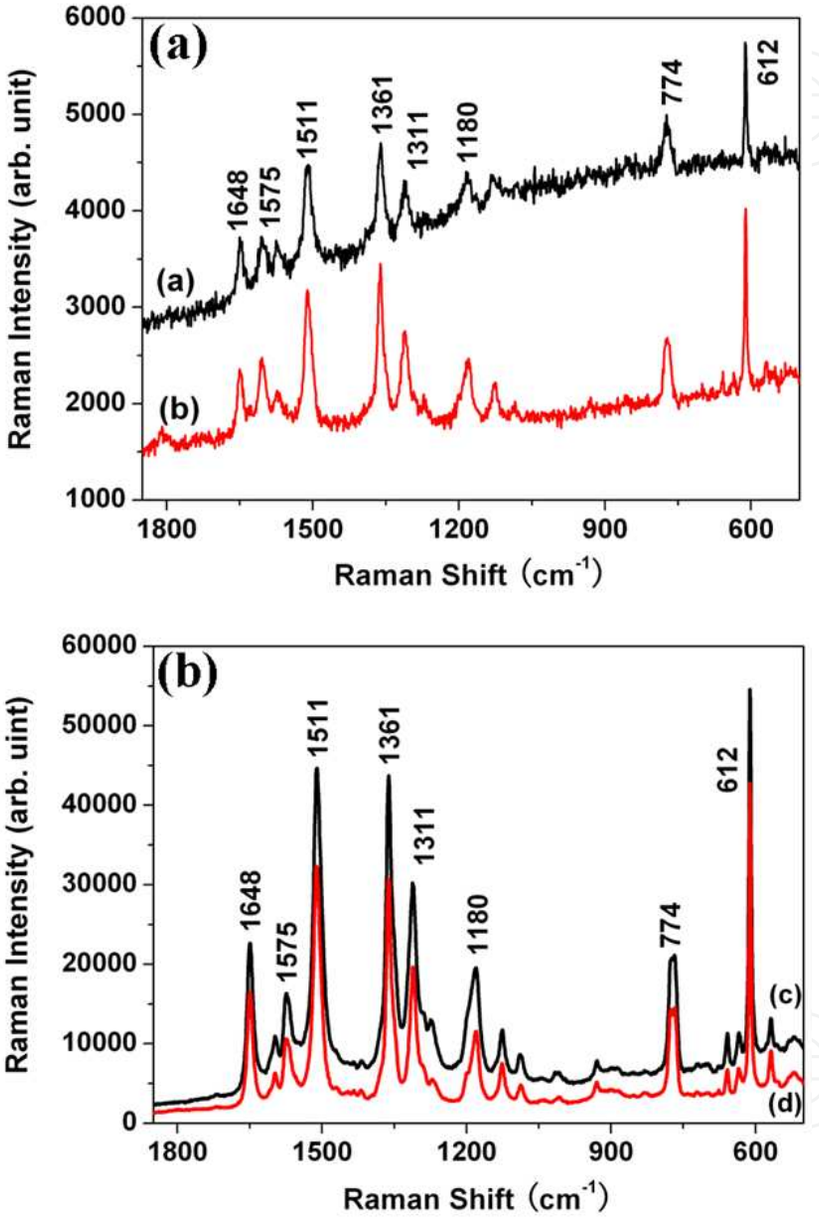

Figure 3. Raman spectra of R6G on thin Ag films consisting of (a) joined nanorods shown by Figs 1(a) (black line) and 1(b) (grey line); and (b) separated Ag nanorods shown by Figs 1(c) (black line) and 1(d) (grey line), respectively, at a concentration of 1×10^{-6}mol/L.

http://dx.doi.org/10.5772/53602

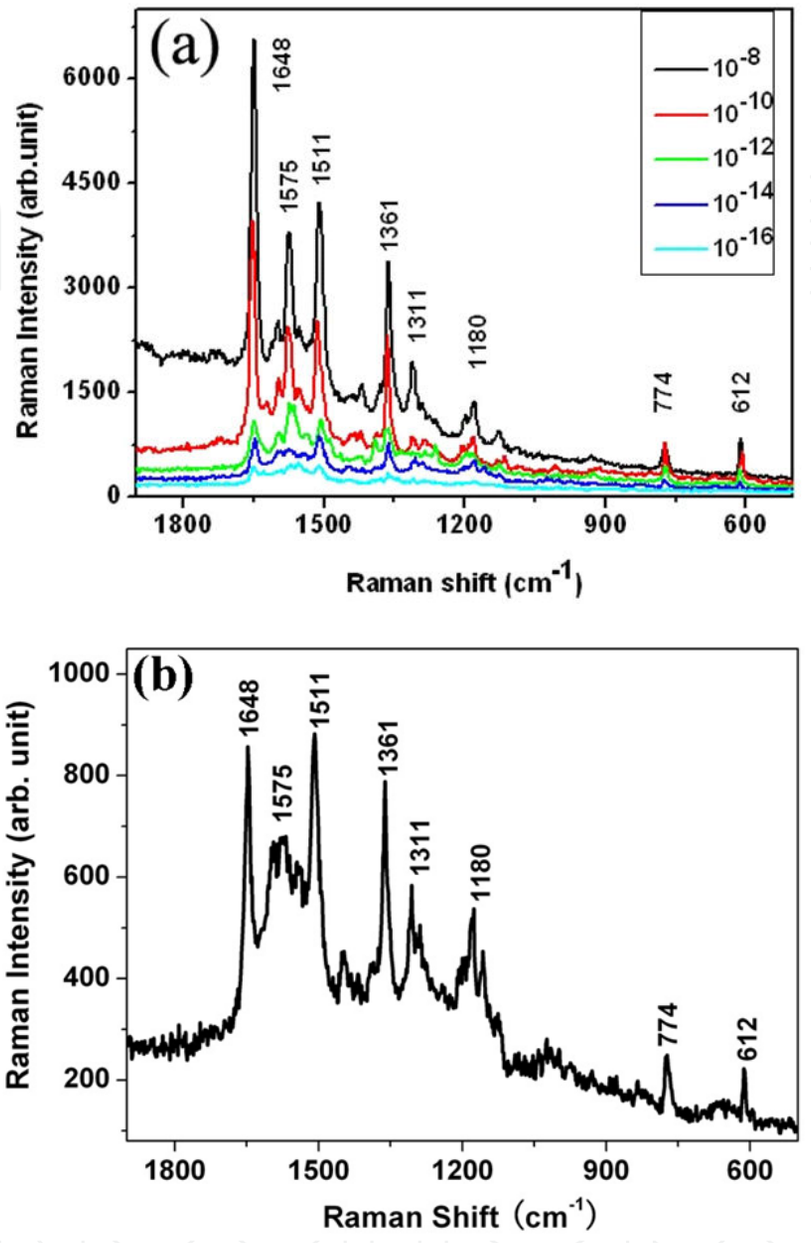

Figure 4. a) Raman spectra of R6G at concentrations ranging from 1×10^{-8} to 1×10^{-16}mol/L; and (b) the Raman spectrum of R6G at a concentration of 1×10^{-14}mol/L, on the thin Ag film consisting of well separated, single crystalline Ag nanorods.

2.2. Enhancement of the sensitivity of SERS substrates via underlayer films

Although the Ag nanorod arrays present sensitive SERS performance, it is still necessary to enable the substrate to detect organic pollutants at trace amount with adequate sensitivity. There are several ways to promote the sensitivity of Ag nanorods as SERS substrates.

Much effort has been devoted to achieving highly sensitive SERS substrates. In particular, multilayer structures can improve SERS enhancement, such as "sandwich" structures with silver oxide or carbon inside and Ag or Au as both underlayer and overlayer [24-28]. Other researchers found that multilayer structures of Ag/Au nanostructures on the smooth metallic underlayer exhibited better SERS sensitivity compared to those without metallic underlayer (EF = 5×10^8) [29-31]. However, the factor that governs the enhancement for multilayer structures is not very clear. Recently, Misra*et al*. obtained remarkably high SERS sensitivity using a micro-cavity with a radius of several micrometers [32]. Shoute*et al*. obtained high SERS signals (EF = 6×10^6) for molecules adsorbed on the silver island films supported by thermally oxidized silicon wafers and declared that the additional enhancement was due to the optical interference effect [33]. All the above experiments and those conducted by Driskell*et al*. suggested that the underlayer reflectivity could play an important role in the multilayer SERS substrates [29].

We have investigated in detail the relationship of underlayer reflectivity and the SERS enhancement of Ag nanorod substrates prepared by oblique angle deposition. We use thin films of different materials with different thicknesses as underlayers to modulate the reflectivity systematically. With the coating of the same Ag nanorods, we find that the SERS intensity increases linearly with the underlayer reflectivity. This conclusion can be explained by a modified Greenler's model we recently developed [34].

To change the reflectivity of the underlayer films, one can vary the dielectric constant and the thickness of the films systematically. We proposed to use Ag, Al, Si and Ti films, since they have different dielectric constants and can be fabricated easily. With a transfer matrix method, we can calculate the reflectivity of those films [35, 36].Fig 5(a) shows the calculated reflectivity spectra of 100 nm Ag, Al, Si, and Ti films. In general, the reflectivity, $R_{Ag} > R_{Al} > R_{Ti} > R_{Si}$, except that at $\lambda \sim 600$ nm where the Si film has a large constructive interference. Fig 5(b) plots the film thickness dependent reflectivity for Ag, Al, Si and Ti at a fixed wavelength $\lambda_0 = 785$ nm. The reflectivity of Ag, Al, Ti, e.g. metals, increases monotonically with the film thickness d. The reflectivity R of Ag, Al and Ti thin films increases sharply when $d <$ 100 nm and almost remains unchanged when 100 nm $\leq d \leq$ 400 nm, while R_{Si} shows an oscillative behaviour due to the interference effect of a dielectric layer.

We deposited thin Ag, Al, Si and Ti films, all with thickness d = 25, 100, and 400 nm, respectively, to achieve different reflectivity. All depositions were carried out in a custom-designed electron-beam deposition system [16].Before the deposition, the glass slide substrates were cleaned by piranha solution (H_2SO_4 : H_2O_2 = 4:1 in volume). The pellets of source materials, Ag, Al, Ti, with 99.99% purity, were purchased from Kurt J. Lesker Company, and Si with 99.9999% purity was purchased from Alfa Aesar Company. The film thickness was monitored *in situ* by a quartz crystal microbalance (QCM) facing toward the vapour source. After the deposition, the reflectivity of the deposited thin films was measured by an Ultraviolet-Visible Spectrophotometer (UV-Vis) double beam spectrophotometer with an integrating sphere (Shimadzu UV-Vis 2450). Fig 5(c) shows the reflectivity spectra of the twelve thin films obtained. The shapes of the reflection spectra are qualitatively consistent with those predicted by the calculations, as shown in Figs. 5(a) and (b). At the same wavelength,

http://dx.doi.org/10.5772/53602

in general, $R_{Ag} > R_{Al} > R_{Ti} > R_{Si}$. In the visible wavelength region, the reflectivity of Ag, Al and Ti increases with the thickness d, while Si demonstrates an oscillating behaviour.

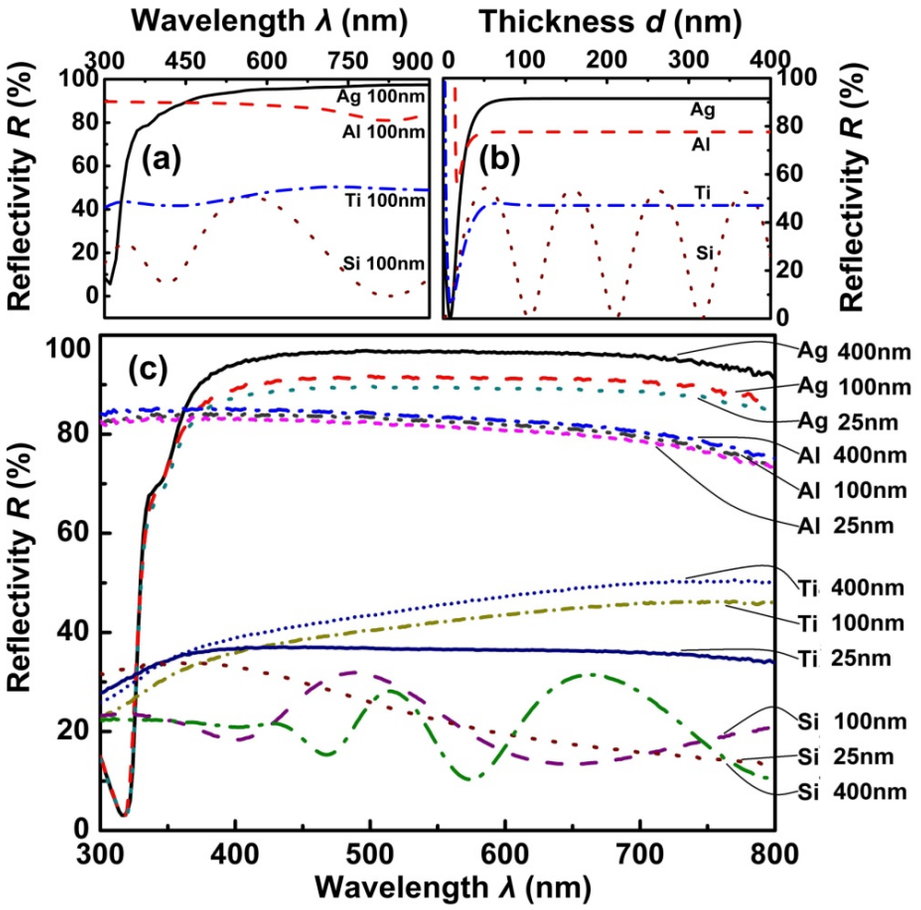

Figure 5. a) Calculated reflectivity R of thin Ag, Al, Si and Ti films at different wavelengths λ with film thickness of 100 nm; b) calculated reflectivity R of thin Ag, Al, Si and Ti films with different thicknesses d at λ_0 = 785 nm; c) experimentally obtained reflectivity spectra of thin Ag, Al, Si and Ti films with different thicknesses.

The twelve deposited planar thin film samples were then loaded into another custom-designed electron-beam evaporation system for Ag nanorod deposition through the so-called oblique angle deposition (OAD) [16, 29, 37].In this deposition, the background pressure was 1×10^{-7}Torr and the substrate holder was rotated so that the deposition flux was incident onto the thin films with an angle $\theta = 86^{o}$ with respect to the surface normal of the substrate holder. The Ag nanorod arrays were formed through a self-shadowing effect [16, 29, 37]. During the deposition, the Ag deposition rate was monitored by a QCM directly facing the incident vapour. The deposition rate was fixed at 0.3 nm/s and the deposition ended when the QCM read 2000 nm (our optimized condition).

The morphologies of the Ag nanorod arrays on different thin film substrates were characterized by a scanning electron microscope (SEM, FEI Inspect F). The typical top-view SEM im-

ages are shown in Fig. 6 and they all look very similar. From the cross-section and top-view SEM images, the length L, diameter D and separation S of these Ag nanorods on different planar thin films are obtained statistically: L_{Ag}= 940 ± 70 nm, D_{Ag}= 90 ± 10 nm, S_{Ag}= 140 ± 30 nm; L_{Al}= 950 ± 50 nm, D_{Al}= 90 ± 10 nm, S_{Al}= 140 ± 30 nm; L_{Si}= 900 ± 50 nm, D_{Si}= 80 ± 10 nm, S_{Si}= 130 ± 20 nm; and L_{Ti}= 930 ± 60 nm, D_{Ti}= 90 ± 10 nm, S_{Ti}= 130 ± 20 nm, respectively. The Ag nanorod tilting angles β were measured to be about 73ºwith respect to substrate normal, which are consistent with our previous results [16, 29, 37]. These structure parameters are very close to one another, implying that the Ag nanorod arrays deposited on different thin film substrates are statistically the same. The SERS response of these Ag nanorod substrates were evaluated under identical conditions: A 2 μL droplet of a Raman probe molecule, trans-1, 2- bis (4-pyridyl) ethylene (BPE) with a concentration of 10^{-5} M, was uniformly dispersed onto the Ag nanorod substrates. The SERS spectra were recorded by the HRC-10HT Raman Analyzer from EnwaveOptronics Inc., with an excitation wavelength of λ_0 = 785 nm, a power of 30 mW and an accumulation time of 10 s.

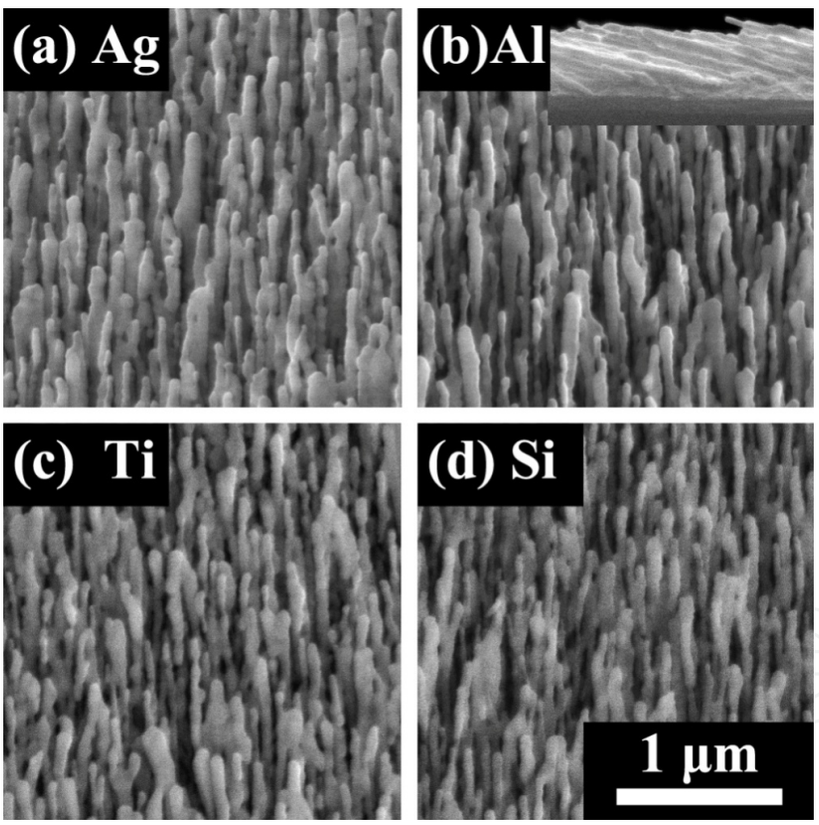

Figure 6. Representative SEM images of Ag nanorod arrays on 100 nm underlayer thin films with different materials: (a) Ag; (b) Al; (c) Ti; (d) Si. All the Figs have the same scale bar.

Fig 7(a) shows the representative BPE SERS spectra obtained at λ_0 = 785 nm from the Ag nanorod arrays on thin Ag, Al, Si and Ti film underlayers (thickness d = 100 nm). Each spectrum is an average of at least 15 different spectra taken at different spots on the substrates. All of them show the three main Raman bands of BPE, $\Delta\nu$ = 1639, 1610, and 1200 cm^{-1}, which

http://dx.doi.org/10.5772/53602

can be assigned to the C=C stretching mode, aromatic ring stretching mode and in-plane ring mode, respectively [38]. The SERS intensity of the Ag nanorods grown on thin Ag film are higher than others and the SERS intensity of the Ag nanorods on Al film is larger than that on Ti film. The Ag nanorods on Si film show the smallest SERS intensity. According to Fig. 5(c), this seems to follow a trend: the larger the underlayer reflectivity, the larger the SERS intensity. To quantitatively compare the SERS response of these substrates, the Raman peak intensity I_{1200} at $\Delta\nu$ = 1200 cm^{-1} is analyzed.

Fig 7(b) plots the SERS intensity I_{1200} versus the reflectivity R of the underlayer thin films at λ_0 = 785 nm. The error bar for the Raman intensity is the standard deviation from 15 or more measurements from multiple sampling spots on the same substrates and the error bar for the reflectivity data is calculated from multiple reflectivity measurements at λ_0 = 785 nm. In Fig. 7(b), the SERS intensity and reflectivity follow a linear relationship: when the reflectivity of the underlayer increases, the SERS enhancement factor increases.

This linear relationship of the underlayer reflectivity and SERS intensity can be explained by a modified Greenler's model developed by Liu *et al*. [34]Greenler's model is proposed through classical electrodynamics to explain the effects of the incident angles and polarization, and the collecting angle on the Raman scattering from a molecule adsorbed on a planar surface [32]. The modified Greenler's model extended the Greenler's model from a planar surface to Ag nanorod substrates and considered the effect of the underlying substrate [34]. The main point of the modified Greenler's model is to consider the conditions of both the incident and scattering fields near the molecule absorbed on a nanorod to calculate the enhancement.

Assuming that relative Raman intensity η is the ratio of the total Raman scattering power to incident light power, according to the modified Greenler's model, η excited by an unpolarized light can be explicitly expressed as [34]

$$\eta = <E^2_{Raman}> \Big/ <E^2_{incident}>$$

$$= \frac{1}{2}\Big\{[1 + R_p + n_2^4 R'_p \cos\delta_p \cos 2(\varphi - \beta) + 2n_2^2 R'^{\frac{1}{2}}_p \cos(\delta'_p + 2\pi\Delta \Big/ \lambda)\sin 2\beta$$

$$+2n_2^2 R_p^{\frac{1}{2}} R'^{\frac{1}{2}}_p \sin 2\varphi \cos(\delta'_p + 2\pi\Delta \Big/ \lambda - \delta_p)](1 + R_p + 2\sqrt{R_p}\cos\delta_p)\cos^2(\varphi - \beta)$$

$$+[1 + n_2^4 R'_s + 2n_2^2 R'^{\frac{1}{2}}_s \cos(\delta'_s + 2\pi\Delta \Big/ \lambda)]\Big\}$$

where R_p and R_s are the reflectivity of *p*- and *s*-polarized lights by the Ag nanorod surface, and R'_p and R'_s are the reflectivity of *p*- and *s*-polarized components by the underlayer thin film; n_2 is complex refractive index of Ag, and n_2 = 0.03 + 5.242*i* (for λ_0 = 785 nm); φ is the light incident angle, and β is the Ag nanorod tilting angle; $\Delta = d\,(1 + \cos 2\varphi) / \cos\varphi$, where d is the thickness of Ag nanorod layer; δ_p, δ_s, δ'_p, and δ'_s are the reflectivity phase shifts of *p*- and *s*-polarization E-fields from Ag nanorods and underlayer thin film, defined as

$$\delta_p = \tan^{-1}[\mathrm{Im}(r_p) \Big/ \mathrm{Re}(r_p)],\ \delta_s = \tan^{-1}[\mathrm{Im}(r_s) \Big/ \mathrm{Re}(r_s)]$$

$$\delta'_p = \tan^{-1}[\mathrm{Im}(r'_p) \Big/ \mathrm{Re}(r'_p)],\ \delta'_s = \tan^{-1}[\mathrm{Im}(r'_s) \Big/ \mathrm{Re}(r'_s)]$$

By setting the light incident angle φ = 0º, the Ag nanorod tilting angle β = 73º, the thickness of Ag layer d = 300 nm, the relative Raman intensity η as a function of the underlayer reflectivity R at λ_0 = 785 nm is calculated and plotted in Fig. 7(c). It shows that the η indeed increases linearly with R, which is in very good agreement with our experimental data shown in Fig. 7(b). Therefore, the underlayer reflectivity is one significant parameter to consider for improving the SERS response of multilayer substrates.

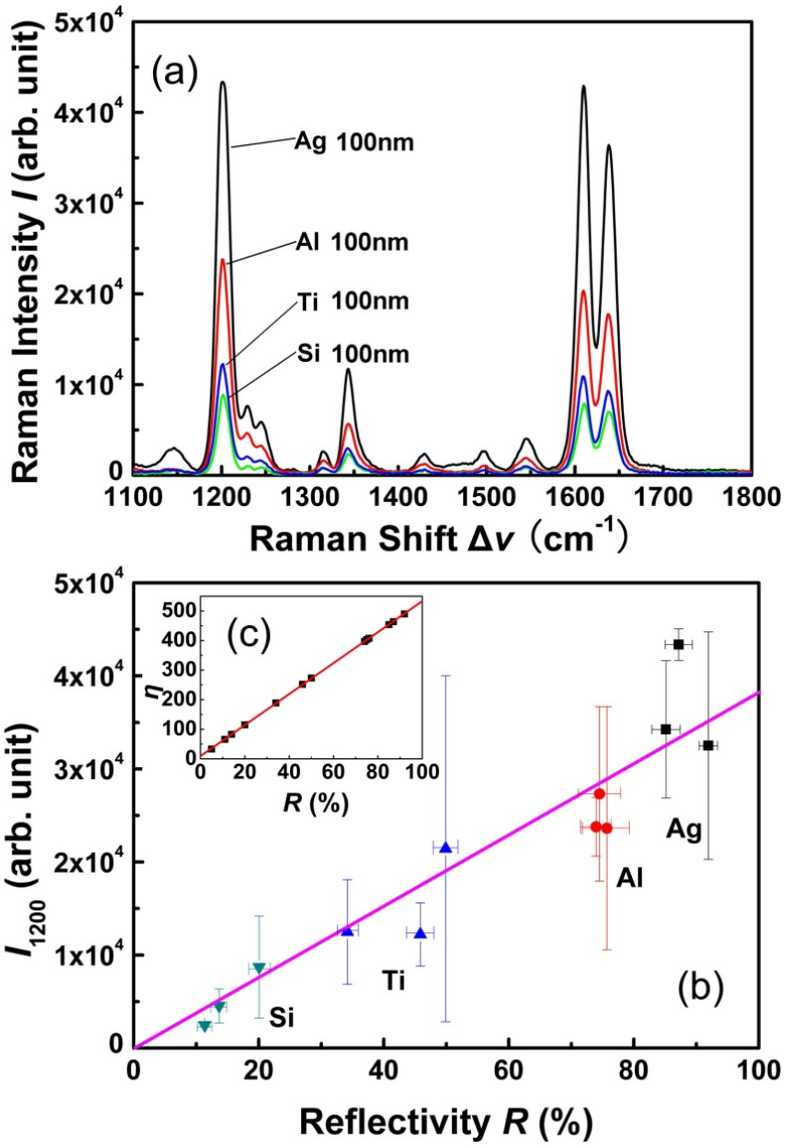

Figure 7. a) BPE SERS spectra obtained from Ag nanorod arrays deposited on 100 nm thin Ag, Al, Si and Ti film underlayers; (b) the plot of experimental Raman intensity as a function of underlayer reflectivity at λ_0 = 785 nm. Different symbol groups represent different kinds of substrates. (c) The plot of the enhanced Raman intensity ratio η as a function of underlayer reflectivity calculated by the modified Greenler's model.

Both our experiments and the modified Greenler's model demonstrate that the higher the underlayer reflectivity, the higher the SERS intensity for the Ag nanorod based SERS sub-

http://dx.doi.org/10.5772/53602

strates. Accordingly, in order to further improve the SERS response of the Ag nanorod substrates, one can further increase the reflectivity of the underlayers through a proper surface coating such as multilayer dielectric coating39.

2.3. Enhancement of the sensitivity from periodical silver nanorods

Most studies have been focused on controlling the morphology of individual nanostructures to maximize their performance as SERS substrates, without consideration of the effect of the ordered arrangement of the nanostructure(s). Obviously, periodically arranged nanostructures might result in an enhancement in the localized electric field due to the resonance with the localized surface Plasmon [40,41] different from that of randomly arranged nanostructures, providing a possibility to improve the performance of SERS substrates. Therefore, it is of great interest to investigate the surface-enhanced Raman scattering from those nanostructures periodically arranged.

The substrates used in the experiment were N-type silicon substrates with an orientation of <100>. Hexagonal lattices (200 μm ×200 μm) of silicon patterns (~ 400nm in diameter) were fabricated on the substrates by electron beam lithography, where the separation distance of the patterns was controlled to be 0 (closely-packed), 50 nm, 100 nm, 200 nm, 300 nm and 400 nm, respectively. These were cleaned in sequence in acetone, ethanol, and de-ionized water baths supersonically, and were mounted on the substrates holder (cooled by liquid nitrogen) in a high vacuum e-beam deposition system (with a background vacuum level better than 2×10^{-5} Pa). Vertically aligned Ag nanorods were deposited on these substrates by the glancing-angle deposition (GLAD) technique described elsewhere [42]. During deposition, the substrate was cooled down to -20 ^{o}C, rotated at a speed of 2 rpm and its surface normal was set ~ 88^{O} off the incoming vapor flux, and the deposition rate was monitored to be ~ 0.5 nm/s using a quartz crystal microbalance.

Oblique-view SEM images is shown from Fig.8 of Ag nanorods deposited on the same silicon substrate fabricated by electron beam lithography, with planar areas, and hexagonal lattice areas (~ 200 μm × 200 μm) of silicon patterns (~ 400nm in diameter) that are separated at 0 nm (closely packed), 50 nm, 100 nm, 200 nm and 300 nm, respectively. Silver nanorods grown on hexagonal lattice areas with other separations are of similar morphology and features. Since the height of silicon micro-patterns etched by electron beam lithography is only ~ 20 nm, there should be also deposition of Ag nanorods in the spaces among the patterns when their separation distance is large enough, e.g., 300 nm, see Fig.8(f). If the separation is not that large, there is normally no deposition of Ag nanorods in these areas because of the shadow effect by the GLAD technique [42]. It is found from the images that Ag nanorods were deposited onto the silicon patterns, forming two-dimensional hexagonal lattices of various lattice parameters (or separation distances of patterns). This provides us ideal samples to investigate the enhancement by the regular arrays to the Raman scattering.

We tested the performance of the hexagonal lattices of patterns covered by Ag nanorods as SERS substrates using R6G as the probing molecule. The samples are dipped in 1×10^{-6} M aqueous solution of R6G for 30 minutes and dried by a continuous gentle nitrogen stream. The Raman spectrum of R6G on each SERS substrate was obtained by measuring and aver-

aging spectra from six different areas of the same hexagonal lattice, by a Reinshaw 100 Raman spectrometer using a 633 nm He-Ne laser as the excitation source. During measurements the spot size of the laser beam was defocused to ~ 10 μm in diameter, and the laser power was decreased to 0.47 mW to avoid any damage to the R6G molecules, signal accumunition time of 10 second per 600 cm^{-1}, 10x objective and NA 0.25. To make a clear comparison of the performance of these SERS substrates, the Raman spectrum of R6G from the unpatterned areas was also measured.

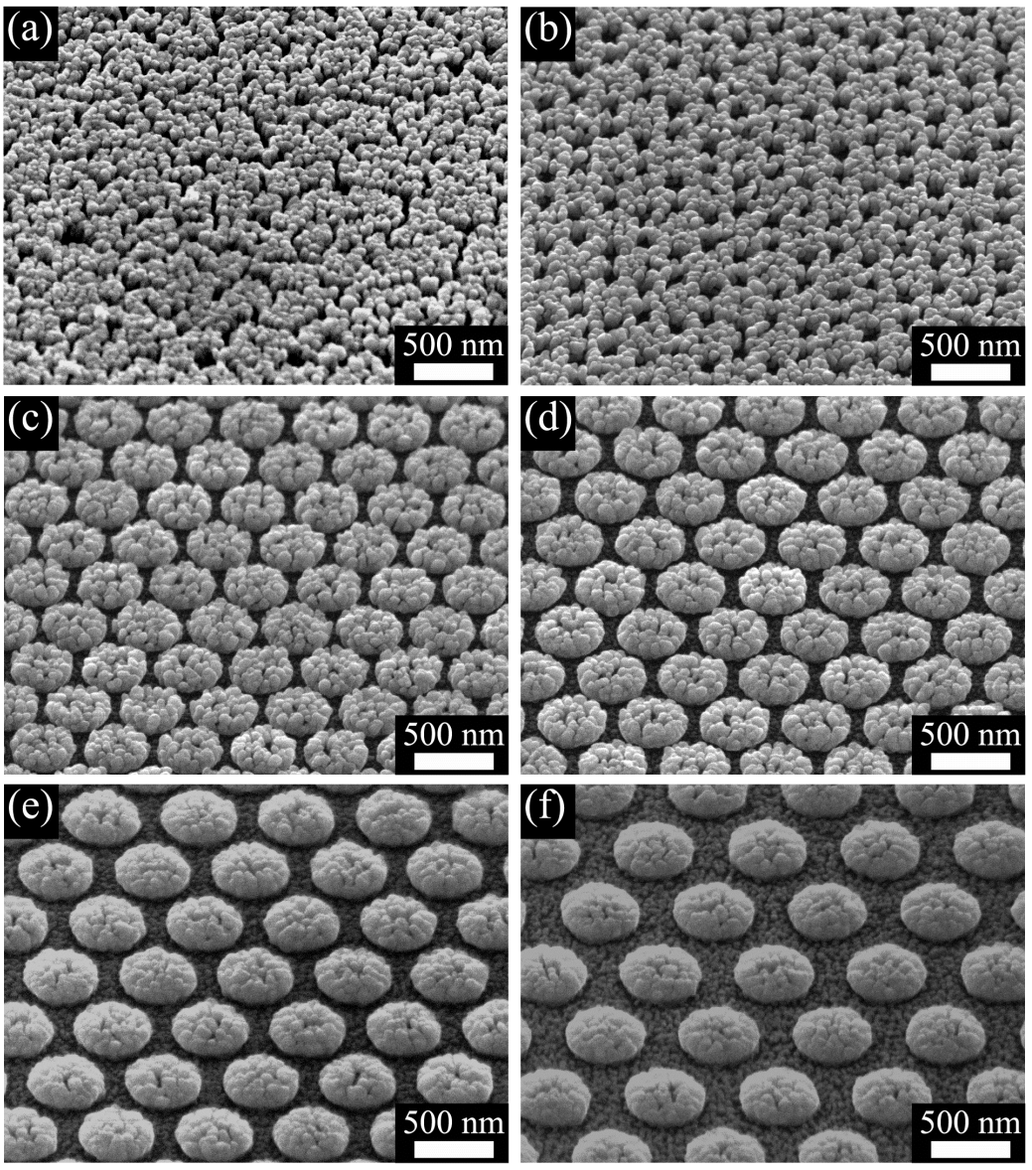

Figure 8. Olique-view SEM images of vertically aligned Ag nanorods deposited on (a) unpatterned silicon; and on hexagonal lattices of silicon patterns that are separated by (b) 0 nm (closely-packed); (c) 50 nm; (d) 100 nm; (e) 200 nm; and (f) 300 nm, respectively.

http://dx.doi.org/10.5772/53602

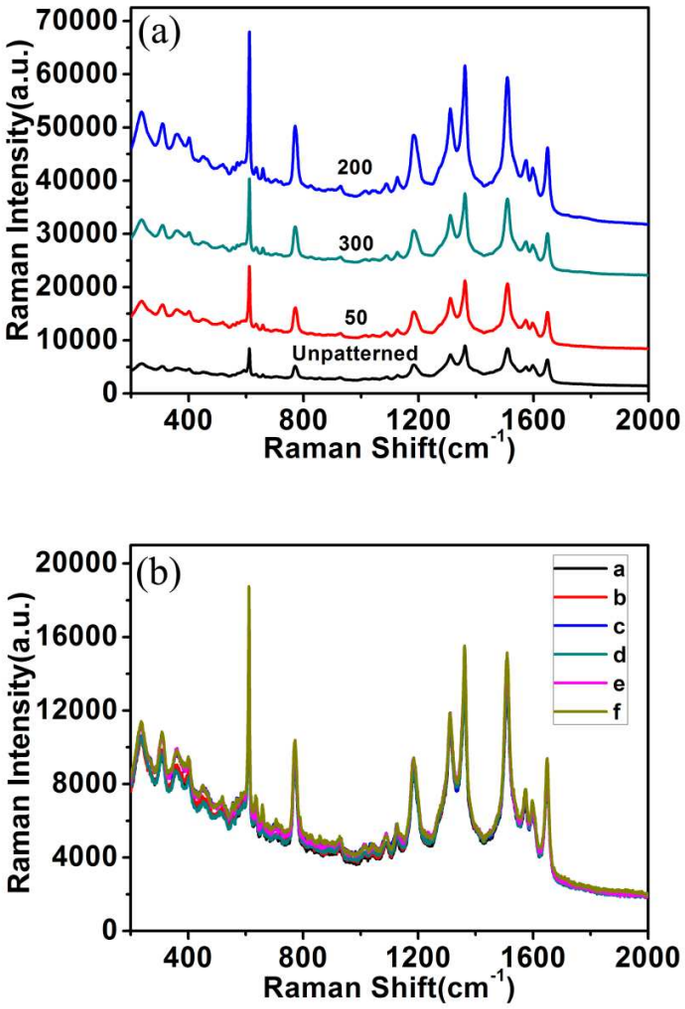

Figure 9. a) Raman spectra of R6G (concentration of 10^{-6} M) using aligned Ag nanorods deposited on unpatterned silicon substrates and on hexagonal lattices of silicon patterns separated by 50, 200 and 300 nm, respectively (To make each spectrum clear, the four spectrum is separated by adding value 0, 6500, 28000 and 14000, respectively), as SERS substrates; and (b) comparison of the Raman spectrum of R6G obtained from six different regions of the hexagonal lattice that are separated at 50 nm of aligned Ag nanorods.

Raman spectra is shown from Fig.9(a) of R6G molecules measured from different areas of the substrate, i.e., the unpatterned area (as the reference), and the hexagonal lattice areas of silicon patterns that are separated at 50 nm, 200 nm and 300nm. We see that each spectrum shows clearly the Raman features of the R6G molecules, and that the signal intensity of the Raman spectrum is very dependent on the substrate (or the separation distance of the patterns). For example, the signal intensity is the highest when the separation distance is 200 nm, and is the lowest in the unpatterned area. Difference in the Raman intensity between the unpatterned area and the hexagonal lattice areas is noticed. Fig.9(b) compares Raman spectra measured from six different areas of the closely-packed lattice, from which one sees that these spectra match quite well. This suggests a good homogeneity of the Raman signals from these SERS substrates.

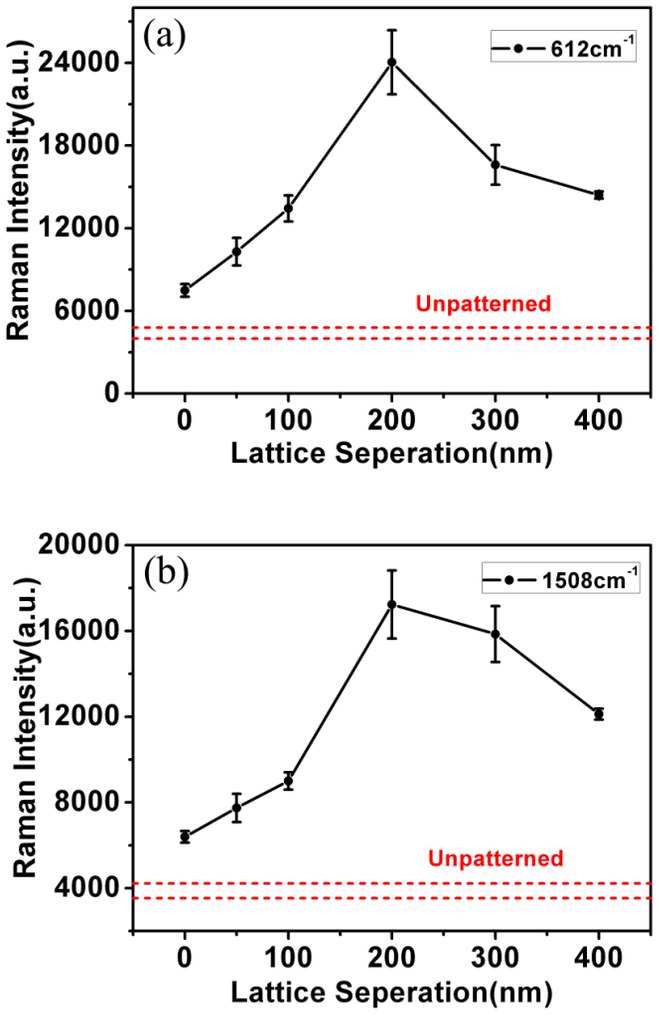

Figure 10. The intensity of the two characteristic peaks of R6G on hexagonal lattices of Ag nanorods: (a) 612 cm^{-1} and (b) 1508 cm^{-1}.

To gain a better understating of the latticing effect on the Raman scattering, we plot the intensity of the two characteristic peaks of R6G molecules, i.e. at ~ 612 cm^{-1} and ~ 1508 cm^{-1}, as a function of the separation distance of the lattice patterns, by comparing with the unpatterned Ag film (the two red dash line represent the sum and difference between the average and uncertainty of signal strength). Fig.10(a) and 10(b) shows respectively the intensity of the two peaks versus the separation distance of the lattice patterns. It is seen from the figures that for the two peaks, they demonstrated very similar dependence behavior on the separation distance. In comparison with signals from the unpartterned area, we notice that

http://dx.doi.org/10.5772/53602

when the patterns are separated at ~ 200 nm, the signals are further enhanced by ~5 times compared with the unpatterned substrates. So the performance of silver nanostructure as SERS substrate is improved through periodical silver nanorods. [43]

3. Detection of PCBs at trace amount by SERS

With the highly sensitive SERS substrates described before, one can detect trace amount organic molecules by the SERS method.

SERS is extremely sensitive in water solutions, for water does not have any Raman peaks. When detecting organic pollutants in nonaqueous systems, we use volatile organic solvents, such as acetone, to dilute pollutants. As the organic solvent shows high Raman background, we need to make the solvent volatilizated completely before SERS measurement.

The powders of 2, 3, 3′, 4, 4′-pentachlorinated biphenyl used in this study were commercially available fromthe AccuStandard Company. Since there is no Raman data of 2, 3, 3′, 4, 4′-pentachlorinated biphenyl reported, we first measured its Raman spectrum and that of acetone, for comparison, see Fig 11(a). To clearly show most characteristic peaks of 2, 3, 3′, 4, 4′-pentachlorinated biphenyl, the Raman spectrum was plotted in two regions of 300 to 1000 cm^{-1} and 1000 to 1700 cm^{-1} respectively, see Figs 11(b) and 14(c). From the Figs one sees that the strongest peaks are located at 342, 395, 436, 465, 495, 507, 517, 598, 679, 731, 833, 891, 1032, 1136, 1179, 1254, 1294, 1573, and 1591 cm^{-1}, respectively; while for acetone the characteristic peaks are at 530, 786, 1065, 1220, 1428 and 1709 cm^{-1}, respectively. It is suggested that 2, 3, 3′, 4, 4′-pentachlorinated biphenyl is distinguishable from acetone and that acetone can be used as the solvent for the SERS measurements, as 2, 3, 3′, 4, 4′-pentachlorinated biphenyl is not soluble in water.

Because the SERS sensitivity is also dependent on the sample treatment, we employed in this study a very simple method to prepare SERS samples, i.e. dropping a small volume (~ 0.5 uL) of solutions of 2, 3, 3′, 4, 4′-pentachlorinated biphenyl in acetone on Ag nanorods using a top single channel pipettor and then blowing away the acetone with a continuous, gentle nitrogen blow. Fig 12(a) shows the Raman spectra of 2, 3, 3′, 4, 4′-pentachlorinated biphenyl dissolved in acetone at concentrations of 10^{-4} to 10^{-10}mol/L, respectively. The accumulation time of each Raman spectrum was 50 seconds and we used only 1% laser power to avoid changing of pentachlorinated biphenyl. When the small volume (~ 0.5 uL) of solutions of 2, 3, 3′, 4, 4′-pentachlorinated biphenyl was dropped on Ag nanorods, it became a circular spot with diameter of about 4 mm. The Raman spectrum was accumulated from a 2 um diameter circular area on the substrates. Therefore, for the solution at concentration of 10^{-10}mol/L, only about ten 2, 3, 3′, 4, 4′-pentachlorinated biphenyl molecules ($2*10^{-23}$mol) would be accumulated in SERS; if that was at concentration of 10^{-8}mol/L, about 1000 molecules ($2*10^{-21}$mol) would be accumulated and so on.

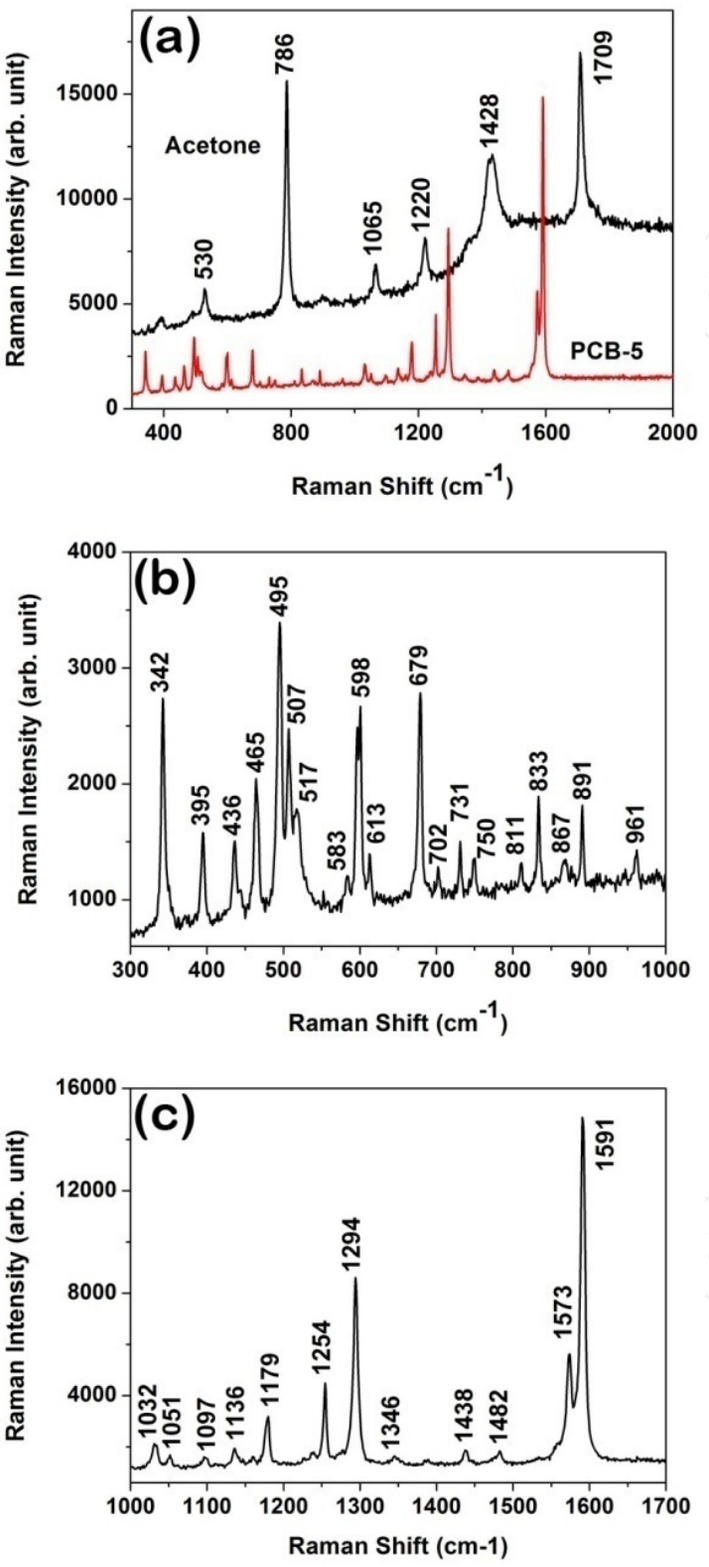

Figure 11. a) Comparison of Raman spectra of PCB-5 powders and acetone; (b) and (c) show details of the Raman spectrum of PCB-5 powders.

http://dx.doi.org/10.5772/53602

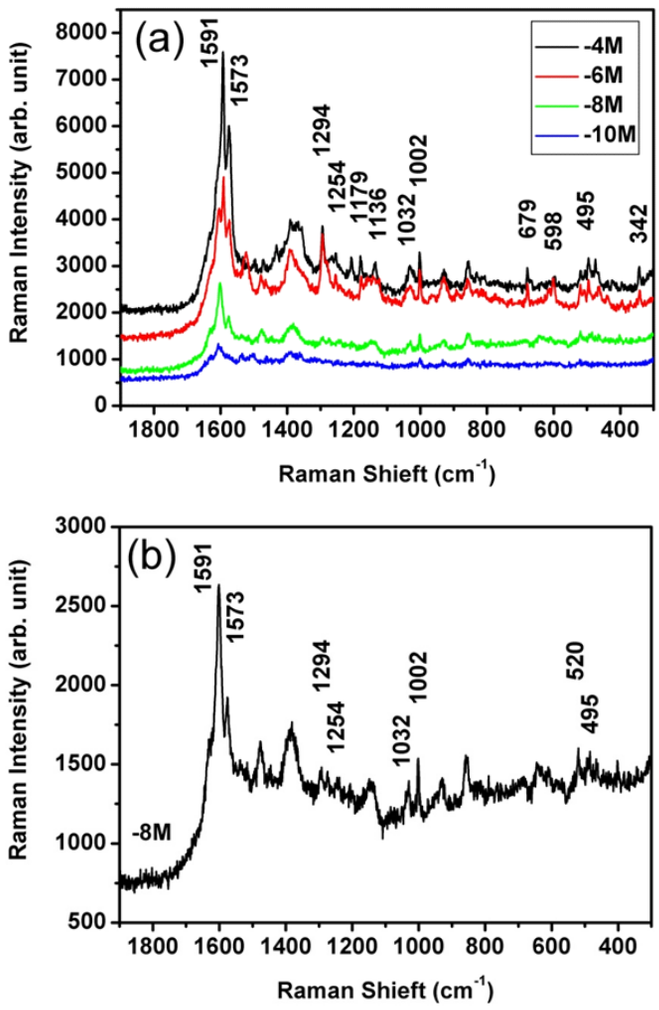

Figure 12. a) SERS spectra of PCB-5 dissolved in acetone with various concentrations; (b) SERS spectrum of PCB-5 in acetone at a concentration of 10^{-8}mol/L.

One sees that the Raman peaks of 10^{-4} mol/L PCB-5 solution located at 342, 495, 598, 679, 1032, 1136, 1179, 1254, 1294, 1573 and 1591 cm^{-1} march the Raman peaks of powder PCB-5 very well, this is quite different from the characteristic peaks of acetone. The peak around 1390 cm^{-1} represents disordered and amorphous carbon on the substrates. Fig 12(b) shows the SERS spectra of 10^{-8} mol/L PCB-5. Peaks located at 495, 1032, 1294, 1573 and 1591 cm^{-1} can march the Raman peaks of powder PCB-5. It indicates that the peaks shown in Fig 12(a) and (b) are the characteristic peaks of dissolved PCB-5, and PCB-5 with a concentration of 10^{-8}mol/L can be detected by the SERS method in the authors' work.

Large scale arrays of aligned and well separated single crystalline Ag nanorods on planar silicon substrate can be fabricated by GLAD method and these Ag films can be used as SERS substrates. With these substrates 2, 3, 3′, 4, 4′- PCB-5 molecules were detected even at a concentration of 10^{-8}mol/L by the SERS method, which indicates that trace amount of PCBs can be detected by the SERS method with Ag nanorods as SERS substrates [44].

4. Detection of POPs at trace level in real environmental samples

In sections 3 we introduced the SERS method to detect trace amount PCBs. In those experiments, the PCBs are in acetone solutions, as fundamental study. In this section we introduce some examples in practical trace POPs detection.

4.1. Detection of PCBs in dry soil samples

The polluted soil samples were dried and made into small powers which were acquired from the Nanjing Institute of Soil (China). With a combination of the high-resolution gas chromatography and mass spectrometry techniques, sample I proved to contain about 5 μg/g PCBs and sample II proved to contain about 300 μg/g PCBs. 0.2 g soil sample I was put into 20 mL acetone and was agitated uniformly for about 5 minutes. This suspension was precipitated for 30 minutes and the transparent acetone solution in the upper layer was taken as solution sample A. 0.2 g soil sample I was put into 200 mL acetone and solution sample B was obtained through the aforementioned process. 0.2 g soil sample II was put into 20 mL acetone to obtain solution sample C and was put into 200 mL acetone to obtain solution sample D.

The Ag nanorods SERS substrates were put into the solution samples A, B, C and D, respectively. After 30 minutes, the Ag nanorods substrates were taken out of the solutions and the acetone on the substrates was blown away using a nitrogen flow. The Raman spectra of these substrates dipped into solution samples were measured by a Renishaw Raman 100 spectrometer using a 633 nm He-Ne laser as the excitation source at room temperature.

Figs 13(a), (b), (c) and (d) show the measured Raman spectrum of the Ag substrates dipped into sample A, B, C and D, respectively. From Figs 13 (a), (b) and (c), one sees peaks at ~1600, 1280, 1240, 1150, 1030 and 1000 cm^{-1} clearly, demonstrating the common feature of PCBs. The peaks around 1590~1600cm^{-1} present benzene stretching vibration mode; the peak around 1280cm^{-1} presents CC bridge stretching vibration mode; the peak around 1030cm^{-1} presents CH bending in-plane mode; the peak around 1000cm^{-1} presents trigonal breathing vibration mode; and peaks around 1240~1250cm^{-1} and 1140~1200cm^{-1} present the vibration peaks induced by Cl substituent. These characteristic peaks suggest that PCBs in dry soil can be detected by the SERS method by dissolving into acetone. The most widely used PCBs are trichlorobiphenyls and pentachlorobiphenyls, we assumed that the molecular weight of the PCBs in the soil samples is 300, then the concentration of the PCBs acetone solution in solution sample A, B, C and D are about 10^{-5}mol/L, 10^{-5}mol/L, 10^{-6}mol/L, 10^{-7}mol/L, and 10^{-8}mol/L, respectively. Thus, with silver nanorod substrates, 5ug/g PCBs in dry soil samples can be detected by the SERS method.

4.2. Detection of PCBs in white spirit

PCBs in white spirit can also be detected by the SERS method with silver nanorod substrates. The concentration of PCBs in white spirit is about 10^{-4}mol/L. We put a drop of PCBs "polluted" white spirit on the silver nanorod substrates and made the white spirit volatil-

http://dx.doi.org/10.5772/53602

ized away. Then, we found PCBs Raman signal with the SERS method described before. Figs 14 (a) and (b) show the SERS spectra of pure white spirit and white spirit with 10^{-4}mol/L PCBs, respectively. One can recognize characteristic Raman peaks of PCBs around 1590, 1290, 1240, 1030 and 1000 cm^{-1} in Fig 14 (b).

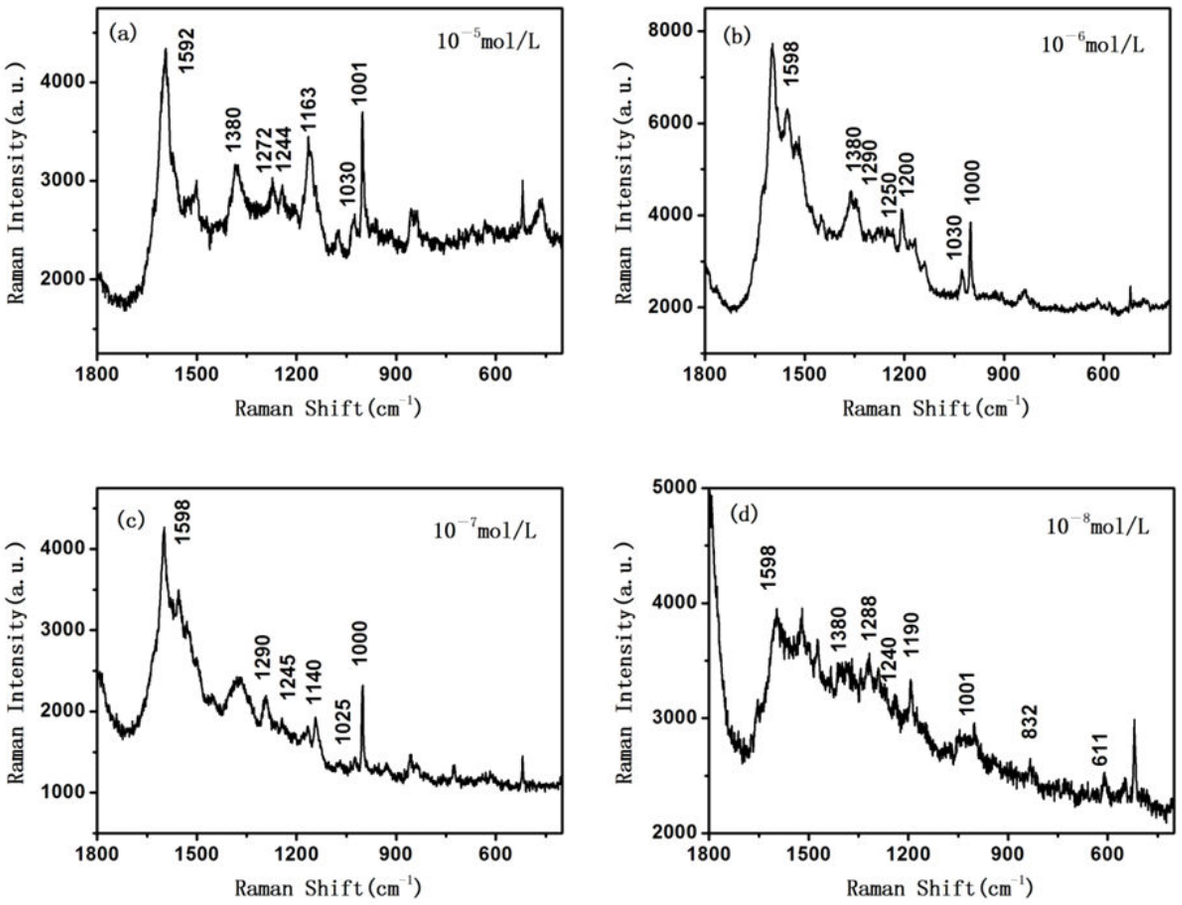

Figure 13. SERS spectra of PCBs in dry soil samples after being treated by acetone: (a) ~10^{-5}mol/L; (b) ~10^{-6}mol/L; (c) ~10^{-7}mol/L; (d) ~10^{-8}mol/L.

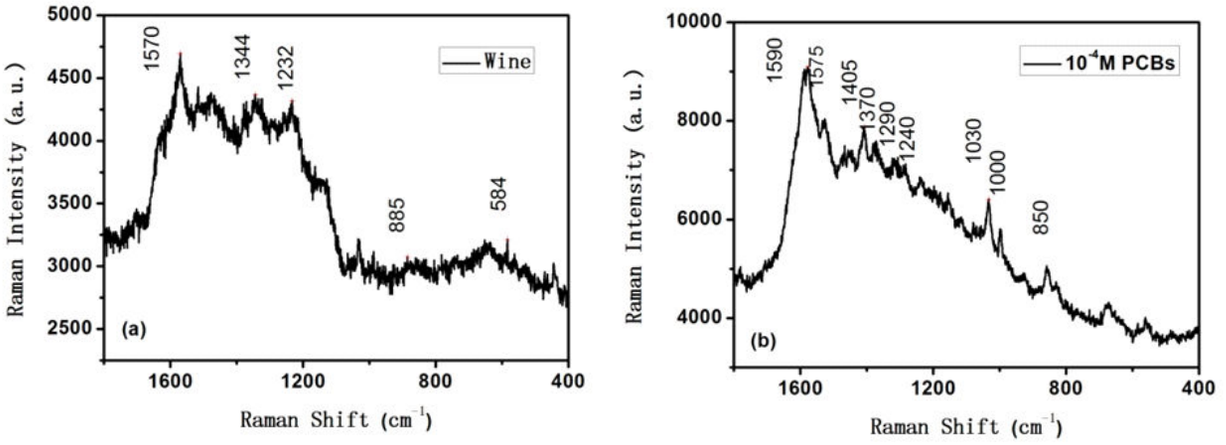

Figure 14. SERS spectra of white spirit without and with PCBs.

4.3. Detection of Melamine in milk

In the year 2009, milk produced by Sanlu Co. (China) was found to contain amounts of Melamine in much higher concentrations than usual. Milk with Melamine seems to contain more protein when detecting nitrogen concentration, but it is poisonous to children. With the SERS method with silver nanorods as substrates, we detected Melamine in milk. Figs 15 (a) and (b) show the SERS spectra of pure Melamine and milk with Melamine.

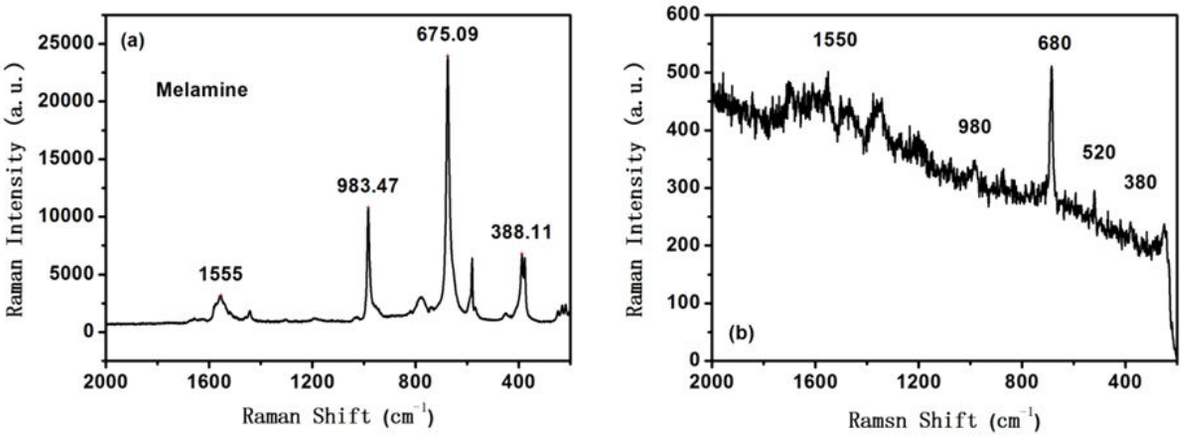

Figure 15. SERS spectra of Melamine and trace Melamine in milk.

5. Summary

In this chapter, it is introduced that although persistent organic pollutants such as PCBs are difficult to detect at trace amount, they can be detected and recognized rapidly via the SERS technique. Ag nanostructured SERS substrates prepared by the glancing angle deposition method are excellent at detection and their sensitivity can be further improved by tuning the thin underlayer films. With well designed and prepared Ag nanostructured SERS substrates, pentachlorinated biphenyl molecules are detected and recognized at trace level using the SERS method. These series of studies provide a potential method for trace pollutant detection via silver nanostructure.

Author details

Zhengjun Zhang[1], Qin Zhou[1,2] and Xian Zhang[1]

*Address all correspondence to: zjzhang@mail.tsinghua.edu.cn

1 Advanced Materials Laboratory, Department of Materials Science and Engineering, Tsinghua University, Beijing, P. R. China

2 Institute of nuclear and new energy technology, Tsinghua University, Beijing, P. R. China

References

[1] Ross G. The public health implications of polychlorinated biphenyls (pcbs) in the environment.Ecotoxicology and Environmental Safety, 2004, 59(3): 275–291.

[2] Ohtsubo Y, Kudo T, Tsuda M, et al. Strategies for bioremediation of polychlorinated biphenyls. Applied Microbiology and Biotechnology, 2004, 65(3): 250–258.

[3] Cicchetti D V, Kaufman A S, Sparrow S S. The relationship between prenatal and postnatal exposure to polychlorinated biphenyls (pcbs) and cognitive, neuropsychological, and behavioral deficits: a critical appraisal. Psychology in the Schools, 2004, 41(6): 589–624.

[4] Hong J E, Pyo H, Park S J, et al. Determination of hydroxy-pcbs in urine by gas chromatography/mass spectrometry with solid-phase extraction and derivatization. AnalyticaChimicaActa, 2005, 531(2): 249–256.

[5] Namiesnik J, Zygmunt B. Selected concentration techniques for gas chromatographic analysis of environmental samples. Chromatographia, 2002, 56Suppl. S: S9–S18.

[6] Pitarch E, Serrano R, Lopez F J, et al. Rapid multiresidue determination of organochlorine and organophosphorus compounds in human serum by solid-phase extrac-

tion and gas chromatography coupled to tandem mass spectrometry. Analytical and Bioanalytical Chemistry, 2003, 376(2): 189–197.

[7] Barra R, Cisternas M, Suarez C, et al. Pcbs and hchs in a salt-marsh sediment record from south-central Chile: use of tsunami signatures and cs-137 fallout as temporal markers. Chemosphere, 2004, 55(7): 965–972.

[8] Moskovits M. Surface-enhanced spectroscopy. Reviews of Modern Physics, 1985, 57(3): 783–826.

[9] Zhou Q, Li Z C, Yang Y, et al. Arrays of aligned, single crystalline silver nanorods for trace amount detection. Journal of Physics D-Applied Physics, 2008, 41(15200715).

[10] Kudelski A. Analytical applications of raman spectroscopy. Talanta, 2008, 76(1): 1–8.

[11] Zhang X Y, Zhao J, Whitney A V, et al. Ultrastable substrates for surface-enhanced raman spectroscopy: al2o3 overlayers fabricated by atomic layer deposition yield improved anthrax biomarker detection. Journal of the American Chemical Society, 2006, 128(JA063876031): 10304–10309.

[12] Tan R Z, Agarwal A, Balasubramanian N, et al. 3d arrays of sers substrate for ultrasensitive molecular detection. Sensors and Actuators a-Physical, 2007, 139(1-2Sp. Iss. SI): 36–41.

[13] Isola N R, Stokes D L, Vo-Dinh T. Surface enhanced raman gene probe for hiv detection. Analytical Chemistry, 1998, 70(7): 1352–1356.

[14] Vodinh T, Houck K, Stokes D L. Surface-enhanced raman gene probes. Analytical Chemistry, 1994, 66(20): 3379–3383.

[15] Tripp R A, Dluhy R A, Zhao Y P. Novel nanostructures for sersbiosensing. Nano Today, 2008, 3(3-4): 31–37.

[16] Chaney S B, Shanmukh S, Dluhy R A, et al. Aligned silver nanorod arrays produce high sensitivity surface-enhanced raman spectroscopy substrates. Applied Physics Letters, 2005, 87(0319083).

[17] Zhang Z Y, Zhao Y P. Tuning the optical absorption properties of agnanorods by their topologic shapes: a discrete dipole approximation calculation. Applied Physics Letters, 2006, 89(0231102).

[18] Malac M, Egerton R F, Brett M J, et al. Fabrication of submicrometer regular arrays of pillars and helices. Journal of Vacuum Science & Technology B, 1999, 17(6): 2671–2674.

[19] Dick B, Brett M J, Smy T. Investigation of substrate rotation at glancing-incidence on thin-film morphology. Journal of Vacuum Science & Technology B, 2003, 21(6): 2569–2575.

[20] Dick B, Brett M J, Smy T J, et al. Periodic magnetic microstructures by glancing angle deposition. Journal of Vacuum Science & Technology A-Vacuum Surface and Films, 2000, 18(4Part 2): 1838–1844.

[21] Alouach H, Fujiwara H, Mankey G J. Magnetocrystalline anisotropy in glancing angle deposited permalloy nanowire arrays. Journal of Vacuum Science & Technology A, 2005, 23(4): 1046–1050.

[22] Singh J P, Tang F, Karabacak T, et al. Enhanced cold field emission from 100 oriented beta-w nanoemitters. Journal of Vacuum Science & Technology B, 2004, 22(3): 1048–1051.

[23] Hawkeye M M, Brett M J. Glancing angle deposition: fabrication, properties, and applications of micro- and nanostructured thin films. Journal of Vacuum Science & Technology A, 2007, 25(5): 1317–1335.

[24] Leverette C L, Shubert V A, Wade T L, et al. Development of a novel dual-layer thick ag substrate for surface-enhanced raman scattering (sers) of self-assembled monolayers. Journal of Physical Chemistry B, 2002, 106(34): 8747–8755.

[25] Li H G, Cullum B M. Dual layer and multilayer enhancements from silver film over nanostructured surface-enhanced raman substrates. Applied Spectroscopy, 2005, 59(4): 410–417.

[26] Li H G, Baum C E, Sun J, et al. Multilayer enhanced gold film over nanostructure surface-enhanced raman substrates. Applied Spectroscopy, 2006, 60(12): 1377–1385.

[27] Yang Y A, Bittner A M, Kern K. A new sers-active sandwich structure. Journal of Solid State Electrochemistry, 2007, 11(2): 150–154.

[28] Mulvaney S P, He L, Natan M J, et al. Three-layer substrates for surface-enhanced raman scattering: preparation and preliminary evaluation. Journal of Raman Spectroscopy, 2003, 34(2): 163–171.

[29] Driskell J D, Shanmukh S, Liu Y, et al. The use of aligned silver nanorod arrays prepared by oblique angle deposition as surface enhanced raman scattering substrates. Journal of Physical Chemistry C, 2008, 112(4): 895–901.

[30] Driskell J D, Lipert R J, Porter M D. Labeled gold nanoparticles immobilized at smooth metallic substrates: systematic investigation of surface plasmon resonance and surface-enhanced raman scattering. Journal of Physical Chemistry B, 2006, 110(35): 17444–17451.

[31] Addison C J, Brolo A G. Nanoparticle-containing structures as a substrate for surface-enhanced raman scattering. Langmuir, 2006, 22(21): 8696–8702.

[32] Misra A K, Sharma S K, Kamemoto L, et al. Novel micro-cavity substrates for improving the raman signal from submicrometer size materials. Applied Spectroscopy, 2009, 63(3): 373–377.

[33] Shoute L, Bergren A J, Mahmoud A M, et al. Optical interference effects in the design of substrates for surface-enhanced raman spectroscopy. Applied Spectroscopy, 2009, 63(2): 133–140.

[34] Liu Y J, Zhao Y P. Simple model for surface-enhanced raman scattering from tilted silver nanorod array substrates. Physical Review B, 2008, 78(0754367).

[35] Mitsas C L, Siapkas D I. Generalized matrix-method for analysis of coherent and incoherent reflectance and transmittance of multilayer structures with rough surfaces, interfaces, and finite substrates. Applied Optics, 1995, 34(10): 1678–1683.

[36] Fu J X, Park B, Zhao Y P. Nanorod-mediated surface plasmon resonance sensor based on effective medium theory. Applied Optics, 2009, 48(23): 4637–4649.

[37] Abell J L, Driskell J D, Dluhy R A, et al. Fabrication and characterization of a multiwell array sers chip with biological applications. Biosensors & Bioelectronics, 2009, 24(12): 3663–3670.

[38] Yang W H, Hulteen J, Schatz G C, et al. A surface-enhanced hyper-raman and surface-enhanced raman scattering study of trans-1,2-bis(4-pyridyl)ethylene adsorbed onto silver film over nanosphere electrodes. Vibrational assignments: experiment and theory. Journal of Chemical Physics, 1996, 104(11): 4313–4323.

[39] Zhou Q, Liu Y J, He Y P, et al. The effect of underlayer thin films on the surface-enhanced raman scattering response of agnanorod substrates. Applied Physics Letters, 2010, 97(12190212).

[40] Brown R. and Milton M., Nanostructures and nanostructured substrates for surface —enhanced Raman scattering. J. Raman Spectrosc. 2008. 39, 1313.

[41] HaynesC L, McFarland A D and Van Duyne R P,Surface-enhanced Raman spectroscopy, Anal. Chem. 2005, 77, 338A.

[42] Zhou Q., Li Z .C., Yang Y. and Zhang Z.J., Arrays of aligned single crystalline silver nanorods for trace amount detection, J. Phys. D Appl. Phys. 2008.41(152007).

[43] Zhang X, Zhou Q, Wang W P, Shen L, et al.Latticing vertically aligned Ag nanorods to enhance its SERS sensitivity.Materials Research Bulletin, 2012, 47,921~924.

[44] Zhou Q, Yang Y, Ni J, et al. Rapid detection of 2, 3, 3 ', 4, 4 '-pentachlorinated biphenyls by silver nanorods-enhanced raman spectroscopy. Physica E-Low-Dimensional Systems & Nanostructures, 2010, 42(5): 1717–1720.

[45] Michaels A M, Jiang J, Brus L. Ag nanocrystal junctions as the site for surface-enhanced raman scattering of single rhodamine 6g molecules. Journal of Physical Chemistry B, 2000, 104(50): 11965–11971.

[46] Mcfarland A D, Young M A, Dieringer J A, et al. Wavelength-scanned surface-enhanced raman excitation spectroscopy. Journal of Physical Chemistry B, 2005, 109(22): 11279–11285.

[47] Qin L D, Zou S L, Xue C, et al. Designing, fabricating, and imaging raman hot spots. Proceedings of the National Academy of Sciences of the United States of America, 2006, 103(36): 13300–13303.

[48] Liu Y J, Zhang Z Y, Zhao Q, et al. Surface enhanced raman scattering from an agnanorod array substrate: the site dependent enhancement and layer absorbance effect. Journal of Physical Chemistry C, 2009, 113(22): 9664–9669.

[49] Gansel J K, Thiel M, Rill M S, et al. Gold helix photonic metamaterial as broadband circular polarizer. Science, 2009, 325(5947): 1513–1515.

IntechOpen